Sustainable Energy: a Bright Future

J. Schoonman[1], D. Perniu[2], and R. van de Krol[1]
[1]Delft Institute for Sustainable Energy
Delft University of Technology
Julianalaan 136, 2628 BL Delft, The Netherlands
[2]Chemistry Department
Transilvania University of Brasov
50 Iuliu Maniu str., 500091 Brasov, Romania
e-mail: j.schoonman@tudelft.nl
e-mail: roxanab@unitbv.ro
e-mail: r.vandekrol@tudelft.nl

1. Introduction

The ever-growing worldwide consumption of fossil fuels and the concomitant emission of greenhouse gases have led to a growing interest in the utilization of renewable energy sources, like, for instance, solar energy, wind energy, biomass, hydropower, and tidal wave energy. However, especially in the fast developing Asian countries, such as China and India, the use of fossil fuels is expected to increase from about 14 million barrels of oil per day to over 30 million barrels per day in 2025 [1]. In addition, Latin America is also experiencing very rapid economic growth that is bringing modern society's environmental problems, including air and water pollution and waste problems to a wider area of our planet. While the limited availability of fossil fuels is also used as an argument to switch to renewable energy sources, it should be kept in mind that supplies of coal could cover the planet's energy demand for more than centuries. But with regard to the reduction of CO_2 emissions, the direct utilization of coal, or hydrocarbons (i.e., natural gas), or in the steam-reforming process to produce hydrogen and the subsequent water-shift reaction to convert the formed CO in the steam-reforming process to CO_2 absolutely requires mineralization, or sequestration of this greenhouse gas [2]. Merkel [3] has discussed the role of science in sustainable development and has stressed that "the key technologies of sustainable development include new energy and propulsion technologies that will help reduce emissions of climate-damaging gases". With regard to emission-free propulsion technologies, a future Hydrogen Economy in which the energy carriers electricity and hydrogen will become interchangeable energy carriers and their combined use may provide a unique pathway towards a decreased dependency on fossil fuels, and reduced greenhouse gas and pollutant emissions. In the long term, hydrogen may play a key role in adapting energy supply to energy demand, as it has the potential for large-scale, even seasonal, energy storage.
The direct conversion of solar energy into electrical energy is very promising, as the world's energy consumption at the turn of the Century was about $4 \cdot 10^{20}$J, while the amount of solar energy reaching the earth is $5.4 \cdot 10^{24}$J per year [4,5]. Indeed, state-of-the-art solar cell technologies have grown in the past few years with overall growth rates between 30% and 40%. Over 85% of the current production is based on silicon wafer, or silicon ribbon technology [6]. Especially in the past few years the price of very pure silicon, required for PV application, is increasing substantially. Hence, novel nano-structured and especially cheaper solar cell materials and innovative devices are being developed.
Electricity from photovoltaic (PV) solar cells or wind energy can be used to produce sustainable hydrogen via electrolysis of water. The direct photo-electrolysis of water is the Holy Grail of Electrochemistry and represents also a materials problem. A major obstacle for the conversion to a Hydrogen Economy is the safe and cheap storage of hydrogen. Nano-structured hydride-forming metals and alloys are attracting global attention to tackle this obstacle.
In this paper, we present an overview of recent studies on nano-structured materials for innovative solar cells, Photo-Electrochemical Cells (PECs), and on hydrogen production and storage.

2. Silicon Photo-Voltaics

The photovoltaic power technology mainly uses silicon-based semiconductor cells. From a solid-state physics point of view, the solar cell comprises a p-n diode with the junction positioned close to the top surface. The principle of this p-n junction device is given in Figure 1.

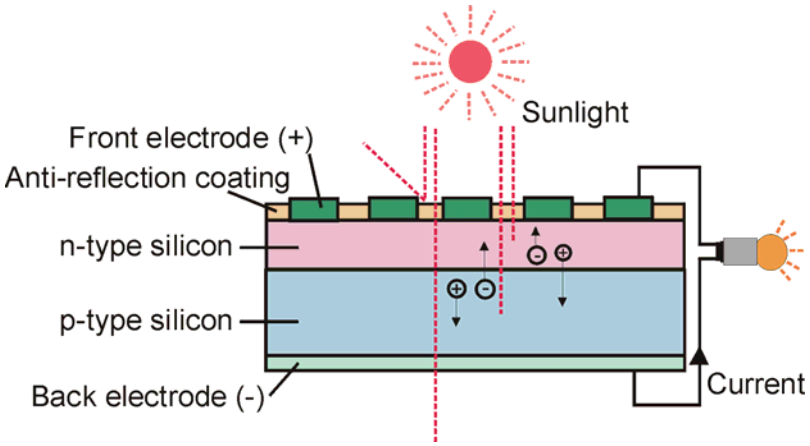

Figure 1. Principle of a silicon-based solar cell.

The solar cell comprises a phosphorus (P)-doped n-type silicon layer connected to a boron (B)-doped p-type silicon layer. The space-charge layer at the p-n junction facilitates the separation of the optically excited charge carriers. The blue colour of the silicon-based PV solar cells is the result of the anti-reflection TiO_2 coating. Depending on the thickness of this anti-reflection coating, gold-coloured or red-coloured silicon-based solar cells can be obtained, but the optimal thickness leads to the blue colour. Several techniques are being employed to characterize the properties of solar cells. One of the most commonly used methods is to measure the current-voltage curves (I-V curves) in dark and under illumination of the solar cell. In Figure 2 an example of a typical I-V curve is presented.

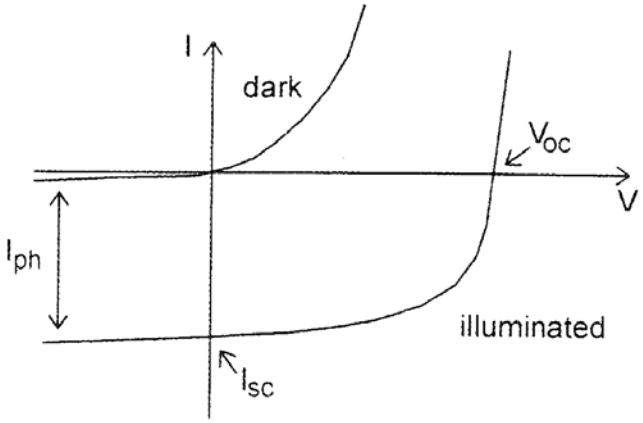

Figure 2. I-V curves for a typical photovoltaic device.

In the dark the I-V curve reveals a diode-type behaviour, which originates from the rectifying nature of the depletion layer near the p-n junction. When illuminated, the diode-type curve is shifted due to the photovoltaic effect, which is characterized by the short-circuit current, I_{SC}, and the open-circuit voltage, V_{OC}. The maximum power point is found by the largest possible rectangle that can be fitted inside the curve under illumination. The fill factor, FF, is a measure of the “squareness” of the curve under illumination and is obtained with Eq. 1,

$$FF = \frac{V_{mp} I_{mp}}{V_{OC} I_{SC}} \qquad (1)$$

in which V_{mp} and I_{mp} are the voltage and the current at the maximum power point, respectively. The FF is a number between 0 and 1. The power conversion efficiency, η, is used as a tool to compare different solar cells and is defined as the percentage of the solar spectrum that is converted into power. It is calculated using Eq. 2,

$$\eta = \frac{V_{OC} I_{sc} FF}{P_{in}} \qquad (2)$$

In which P_{in} is the incoming power of the used white light source. To make a correct comparison possible, all measurements should be carried out under the same circumstances, using the same spectral distribution and intensity of the light source, and at the same temperature. For this reason international standard test conditions are set in literature. Cells should be measured at 25°C, with a radiant intensity of 1000 W/m^2 and a spectral distribution comparable to the (direct and diffuse) spectrum of the sun in the earth atmosphere at an angle of 48.2°. This is called the AM 1.5 global spectrum and is available using commercially available solar simulators [14].

3. Solar Cell Categories

Solar cells can be divided into several categories. These are, including the efficiency of commercial cells and the efficiency obtained in the Laboratory, respectively: Single-Crystalline Si (13-16%, 24.7%), Polycrystalline Si (12-15%, 19.8%), Amorphous Si (4-7%, 10.1%), III-V GaAs, (Ga)InP (21%, 25%), II-VI CdTe, ZnSe, CdS (5%, 16.5%), I-III-VI $CuInS_2$, $Cu(In,Ga)(S,Se)_2$ (in combination with ZnO, or CdS) (12%, 19%), Dye-Sensitized (7%, 11.4%), and the Solid-State Nano-Structured Heterojunction, for which only the laboratory conversion efficiency has been established, i.e., 5.4%. Microcrystalline and proto-crystalline Si are also recently under development for PV solar cells.
It is seen that several of the new solar cell materials are based on cadmium (Cd), arsenic (As), or selenium (Se), which are not environmentally acceptable. In addition, GaAs-based devices are very expensive. These are used in space applications. Here, we will focus on the Dye-Sensitized and the Solid-State Nano-Structured Heterojunction solar cells.
Nano-structured materials are distinguished from conventional polycrystalline materials by the large fraction of grain boundaries in bulk materials, and hence a large percentage of surface atoms in the bulk of a material. In nano-structured materials surface properties start to determine bulk properties, but also ions further away from the surface experience modified conditions, due to space-charge layer formation, which is considered an intrinsic effect of the nano-size, in contrast to the surface effects, which are considered extrinsic effects of the nano-size. Accordingly, material constants that used to be considered as inaccessible to engineering have become susceptible to human manipulation, hence tailoring of fundamental material properties has become possible.

4. The Grätzel Solar Cell and Beyond

A novel way to harvest solar energy is based on a photo-electrochemical (PEC) approach, in which the essential region is the interface between an n-type semiconductor and a liquid electrolyte. Regenerative PEC cells produce electrical energy, but the PEC cell can also generate a chemical fuel, i.e., hydrogen, through the photo-cleavage of water [7]. The potential applications of PEC cells for solar energy conversion by water splitting to form the energy carrier hydrogen were recognized some three decades ago by Fujishima and Honda [8], who used a single-crystalline rutile TiO_2 photo-anode. This material is, due to its band gap energy of 3.2 eV, only sensitive to the near UV part of the solar spectrum. Unfortunately, highly efficient PEC cells based on Si or GaAs, which absorb the visible part of the solar spectrum efficiently, suffer from passivation by the formation of a SiO_2 layer, or by dissolution of GaAs under visible-light irradiation, respectively.
An alternative approach is to use a stable semiconductor, which exhibits a low solar light-to-electrical conversion efficiency, like TiO_2 or ZnO, and to sensitize this material with a visible-light absorbing dye. The sensitization of rutile-structured TiO_2 and $SrTiO_3$ by visible light has been demonstrated already by Mackor and Schoonman in 1980 [9]. However, they used single-crystalline materials and thick layers of the visible-light absorbing dyes, while more recent research indicated that only one monolayer of the dye molecule is able to inject an excited photo-electron into the conduction band of TiO_2. The practical use of sensitized flat surfaces in regenerative, electricity

producing PEC cells is, however, limited by the low light-harvesting efficiency obtained with a single monolayer of a dye molecule. The absorption of a monolayer of a dye molecule is weak, because the area occupied by one molecule is much larger than its optical cross section for light capture. An improved PV efficiency, therefore, cannot be obtained by the use of a flat semiconductor surface, but rather by the use of a highly porous, nano-structured film of very high surface roughness. Hence, a large number of dye molecules, as present as a monolayer, is available for visible-light absorption, because of the large surface area of the nano-structured film. A major breakthrough is the dye-sensitized solar cell, reported by Grätzel and co-workers [7,10,11]. This dye-sensitized solar cell is schematically presented in Figure 3.

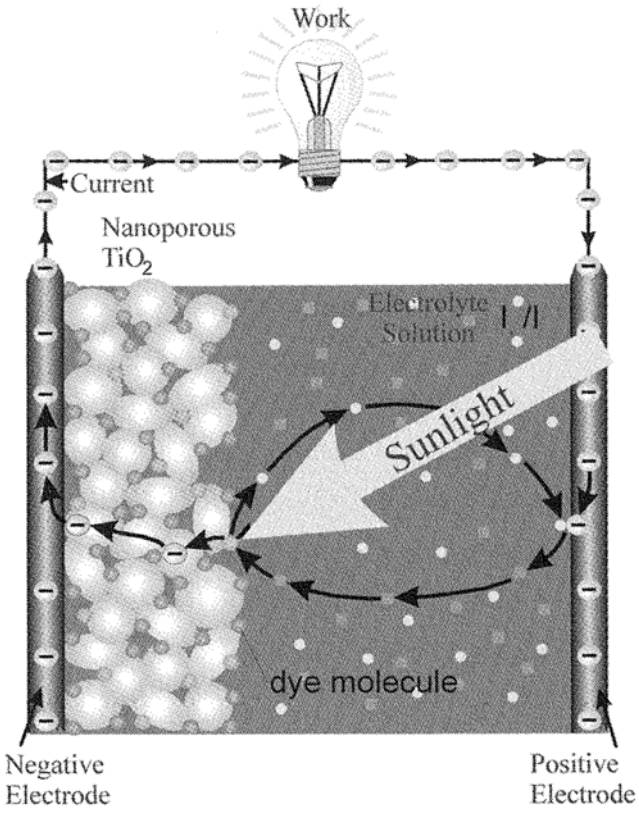

Figure 3. Schematic presentation of the dye-sensitized Grätzel solar cell [10,11].

The wide-band gap nano-porous anatase-structured TiO_2 with primary particle sizes in the order of 20 to 50 nm is covered with a monolayer of a visible-light absorbing dye molecule, usually an organo-metallic ruthenium complex [10,11]. Visible light is absorbed by the dye molecule, exciting an electron from the highest occupied molecular orbital (HOMO) to the lowest unoccupied molecular orbital (LUMO) of the dye molecule. Because the energy of the excited state is above the conduction band edge of TiO_2, the photo-excited electron can be injected into the conduction band of the nano-structured TiO_2 and percolates via the interconnected TiO_2 nano-particles to the back electrode, usually a transparent metallic conducting transparent metal oxide (TCO) electrode, like indium-tin oxide, or fluoride-doped tin oxide on a glass substrate. At a TCO-counter electrode, an iodide/iodine redox couple dissolved in the liquid electrolyte acetonitril, mediates the electron to the oxidized state of the dye molecule, thereby closing the electrical circuit by regeneration of the dye molecule. The maximum voltage that such a device can deliver corresponds to the difference between the redox potential of the mediator and the Fermi level of the n-type semiconductor. The conversion efficiency of the dye-sensitized Grätzel solar cell is at present 11.4% [12].
The presence of a liquid electrolyte in the Grätzel solar cell has stimulated investigations to arrive at a three-dimensional (3D) all solid-state alternative of the Grätzel solar cell. The combination of the adsorbed monolayer of the dye molecule on the nano-structured n-type TiO_2 and the liquid electrolyte with the iodide/iodine redox couple has been replaced by a visible-light absorbing p-type organic or inorganic semiconductor. Huisman et al. [13,14] have investigated the combination of porous nano-structured n-type anatase-structured TiO_2 with a primary particle size of about 50nm in combination with spin-casted poly(3-octyl)thiophene (P3OT). Cell characteristics of devices with a

300 nm film of TiO_2 and an equivalence of 30 nm P3OT inside the pores are a short-circuit current density of 0.25 mA/cm^2, an open-circuit voltage V_{OC} of 0.72V, a Fill-Factor of 0.35, and a conversion efficiency of 0.06%, using white light with an intensity of 1000 W/m^2 (not AM 1.5). The Incident Photon to Current Conversion Efficiency (IPCE) was only 2.5% at 488nm, while it is larger than 85% for the Grätzel solar cell.

Van de Krol and Perniu et al. [15] have described thin-film techniques for novel three-dimensional (3D) solid-state solar cells, i.e., Chemical Vapour Deposition (CVD) and Atomic Layer Deposition (ALD). CVD is very beneficial for the manufacture of the Extremely-Thin Absorber (ETA) solar cell [16] and ALD for TiO_2-$CuInS_2$ 3D hetero-junction solar cells.

While in CVD all precursors are introduced into the deposition chamber at the same time and process conditions are selected such as to deposit smooth or structured layers, in Atomic Layer Deposition (ALD) the precursors are introduced into the deposition chamber sequentially. This leads to a self-limiting growth mechanism while gas-phase reactions are inhibited due to the sequential introduction of the precursors. By carefully tuning the relevant process parameters, i.e., pulse length, reactor chamber pressure, deposition temperature, and number of deposition cycles, thin films of high purity and a well-defined thickness are obtained [4, 20].

The 3D hetero-junction solar cells and their manufacture have been reported by Nanu et al. [17,18]. Highly porous, nano-structured anatase TiO_2 layers are the basis of the 3D TiO_2-$CuInS_2$ hetero-junction solar cells. Here the nano-sized pores of the near-UV absorbing n-type substrate are infiltrated with the visible-light absorbing p-type $CuInS_2$ using ALD to form the 3D solar cell. Figure 4 presents this hetero-junction solar cell.

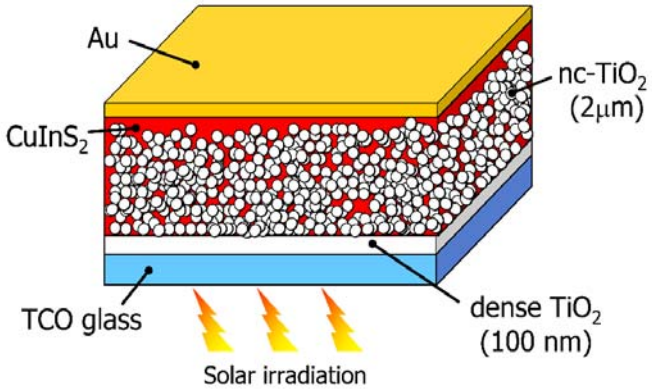

Figure 4: Structure of the inorganic 3D hetero-junction solar cell.

As is shown in Figure 5, this type of solar cell exhibits an open-circuit voltage of 0.53V, a short-circuit current of 20.6 mA/cm^2, a FF of 0.5, and an overall conversion efficiency of 5,4%, all measured under AM 1.5 irradiation from a calibrated solar simulator [18].

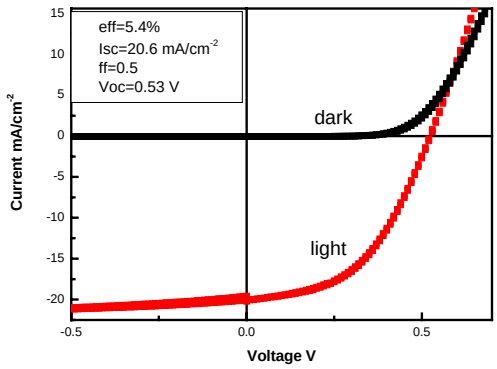

Figure 5. I-V curves in dark and under illumination [17,18].

Recently, Huisman et al. [19] have reported the application of inverse titania (TiO_2) opals in nano-structured solar cells [19]. Periodicity on an optical length scale leads to materials that exhibit a full photonic band gap, i.e., a wavelength band in which photon propagation is forbidden. Usually, the

building blocks for photonic crystals (opals) are monodispersed colloids. Next to periodicity with a well-chosen lattice spacing, also a high porosity and a high refractive index are prerequisites to obtain a photonic band gap. This is achieved by inversion of the opals, using infiltration, followed by removal of the template by calcination. In this way inverse photonic crystals (inverse opals) are created, which comprise a periodic structure of air voids in a solid-state matrix. Huisman et al. [19] have used inverse TiO_2 opals to study a solar cell based on the Grätzel-type solar cell, using the Ru 535-dye and as electrolyte a solution of I_2/I^- in propylene carbonate, and a solid-state cell that contains poly(3-octylthiophene) (P3OT), which is infiltrated in the pores by spin casting a P3OT solution or by melting. The parameters for the solar cell with the Ru-dye are V_{OC}=0.56V, I_{SC}=1.8mA/cm^2, FF=0.6, and an efficiency of 0.6%. For the solar cell that contains P3OT these parameters are 0.58V, 0.2mA/cm^2, 0.25, and 0.03%, respectively. Poor charge-transfer characteristics of P3OT in this cell configuration cause the deterioration of the solar cell, compared to the Ru-dye containing cell. It is however clear that the efficiency of the investigated solar cells needs to be increased substantially. This can be achieved by increasing the ordered portions of the nanoporous TiO_2 network [19] and, therefore, the optimisation of inverse opals are attracting increased attention.

5. Photo-electrolysis

While silicon-based and the novel 3D solar cells can, in principle, be coupled to a commercial electrolyser to split water into oxygen and the energy carrier hydrogen, the direct photo-electrolysis of water could be a more efficient route to especially small-scale decentralised production of sustainable hydrogen. Especially, the prospect of a future Hydrogen Economy has intensified interest in the photo-catalytic splitting of water. Since the pioneering research of Fujishima and Honda [8], many photo-electrode materials have been investigated, but with minor success, and, therefore, the wide-band gap transition metal oxides, in particular anatase-structured TiO_2, have attracted widespread attention, because of intrinsic high photochemical stability. Anatase-structured TiO_2 has to be sensitized for visible light though, as it absorbs only the near UV part of the solar spectrum. Usually, transition-metal oxides are used as dopants as they introduce energy levels in the band gap, thus making sub-band gap excitation of electrons into the conduction band of TiO_2 possible. For instance, the small sub-band gap photocurrents observed for Fe-doped anatase-TiO_2 can be explained by Fe^{3+} dopant ions, which introduce strongly localised d-state energy levels deep in the band gap, i.e., just above the valence band and which lead, besides to recombination, to hopping of the electron holes over these localised energy levels [21]. The diffusion of electron holes in the valence band is much faster, compared to this hopping mechanism. Besides cation doping, anion doping is being investigated recently. Asahi et al. have shown that anion dopants N, C, S, P can also be used to sensitise TiO_2 to visible light [22]. The p-orbitals of these anions exhibit significant overlap with the valence-band O-2p orbitals, which facilitates the transport of photo-generated electron holes to the surface of the photo-anode [22]. Enache et al. have investigated for the first time the photo-electrochemical properties of carbon-doped anatase-structured TiO_2 [21]. While virtually no photocurrent has been observed in the visible part of the solar spectrum, which was attributed to a (too) low carbon content, the photocurrent due to band-to-band excitation was significantly higher than that of undoped TiO_2, despite the high donor density and correspondingly small depletion layer in C-doped anatase-structured TiO_2. The origin of the enhanced photocurrent is most likely a change in the electronic structure of the material due to the incorporation of carbon and/or related point defects. Regarding the synthesis procedure, i.e., spray pyrolysis under a mixed CO_2/O_2 atmosphere [21], carbon incorporation into the lattice may be in the form of carbonate anions, where carbon will occupy a titanium-ion lattice site, in contrast to anion-doping. Detailed studies of the defect chemistry of anion-doped anatase-structured TiO_2 are necessary to unravel the photo-catalysis mechanisms.

An innovative materials concept for a photo-anode is based on the 3D nano-structured solid-state solar cell, presented in Figure 4. While this solar cell is based on the visible-light absorbing p-type conducting chalcopyrite $CuInS_2$ and the near UV-absorbing anatase-structured TiO_2 in a 3D nano-structured array of p-n junctions, the novel concept comprises a photo-anode in the form of a laminar array of a thin film of (cation, or anion)-doped TiO_2 and $CuInS_2$. The concept is presented in Figure 6.

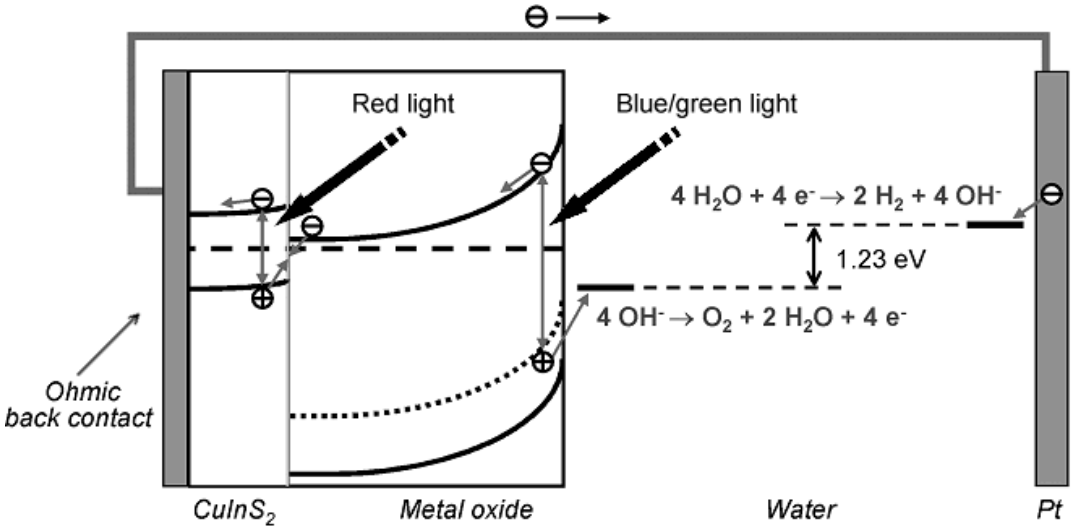

Fig. 6. The Delft Multi-Junction Photo-Electrochemical Cell (PEC) [15].

This multi-junction photo-anode comprises doped anatase-structured TiO_2 and $CuInS_2$, which absorb near UV/blue/green light and green/yellow/red light, respectively. The doped n-type metal oxide also acts as a protective optical window for the p-type absorbing $CuInS_2$ layer. From the energy band structure of this laminar photo-electrode, it is apparent that the visible-light absorbing $CuInS_2$ layer between the current collector, comprising a Transparent-Conducting Oxide (TCO, usually indium-tin oxide, or fluoride-doped tin oxide) and the layer of doped TiO_2, facilitates increased photo-electron transport to the counter electrode. This photo-anode, at which oxygen is formed, is currently being investigated in depth in the Delft Institute for Sustainable Energy in order to arrive at an optimal photo-electrochemical cell for the direct formation of sustainable hydrogen by splitting of water under solar irradiation.

6. The Hydrogen Economy

The Hydrogen Economy is an economy, in which hydrogen (H_2) is used as an energy carrier. To date, hydrogen is produced on an industrial scale using the steam-reforming process, followed by the water-shift reaction. Usually, natural gas (methane, CH_4) is used and the following reactions describe in principle the industrial process.

Steam reforming of natural gas:

$$CH_4(g) + H_2O \xrightarrow[2.5bar]{850°C} CO(g) + 3H_2(g) \qquad (3)$$

Water-shift reaction:

$$CO(g) + H_2O \xrightarrow{350°C} CO_2 + H_2(g) \qquad (4)$$

Industrial production rates are up to 100.000 m^3/hour. Besides the steam-reforming process to produce hydrogen using natural gas, the electrolysis of water to form hydrogen and oxygen is commercially used. The electrolyte has a composition based on pure water with an electrical conductivity of less than 5 μ S/cm and to which 30% potassium hydroxide (KOH) is added. The pure water is necessary in order to avoid impurity metal deposition on the cathode. The electrolysis reactions of this alkaline solution are:

Anode: $4\ OH^- \rightarrow O_2 + 2\ H_2O + 4e^-$ (5)

Cathode: $4\ H_2O + 4e^- \rightarrow 2\ H_2 + 4\ OH^-$ (6)

- -

Overall: $2\ H_2O \rightarrow 2\ H_2 + O_2$ (7)

Electrolysis is performed at 1 bar and 1.76 volt.
If the electrical energy for the electrolysis of water originates from photovoltaic conversion of solar energy, for example, using silicon-based or advanced solar cells, or from wind energy, the produced hydrogen is referred to as "Sustainable Hydrogen".

The current research and development activities are focused on the production of hydrogen using the clean-fossil fuel approach, or using sustainable energy sources. The clean-fossil fuel approach is based on the conversion of hydrocarbons with steam at high temperatures and subsequent sequestration or mineralization of the produced CO_2, while the use of sustainable energy sources, like solar and wind energy in combination with an electrolyser, or, the direct photo-electrolysis, for the splitting of water leads to CO_2-free hydrogen as described in the previous section. Furthermore, the safe storage of hydrogen, its conversion to electrical energy using fuel cells, and the safety aspects in relation to social acceptance attract widespread attention.
Hydrogen, as an energy carrier, is based on the chemical reaction:

$H_2(g) + ½O_2 \rightarrow H_2O(l) + 286$ kJ/mole (8)

Hydrogen is the 3rd abundant element on earth, it has no toxic reaction products like CO, CO_2, NO_x, SO_x,etc, is sustainable and renewable and the question then arises as to whether hydrogen could meet today's energy demands? At the turn of the century the global energy demand amounted to 4.10^{20} J/year. With respect to hydrogen 1 GJ can be obtained per 90 liters of water. Therefore, the amount of water needed is $3.6.10^{13}$ liters. The oceans contain $1.45.10^{21}$ liters of water and the annual rainfall amounts to $3.62.10^{17}$ liters. Hence, there is enough water to sustain a Hydrogen Economy.
A very important issue will be the social acceptance of hydrogen as an energy carrier. It is, therefore, of utmost importance to inform society of the properties of hydrogen in relation to safety. How (un)safe is hydrogen? It is not decomposing, not self-igniting, not fire-supporting, not toxic, not corrosive, not radioactive, not badly smelling, not contagious, not polluting water, no danger to unborn children, and not carcinogenic. Hydrogen is lighter than air and moves rapidly upwards and dilutes very fast (high diffusion coefficient), it has tight explosion limits and when ignites early, and it burns before explosion limits are reached. The dramatic Hindenburg accident was not caused by hydrogen, but by the flammable mantle material of this zeppelin. In addition, a cheap and safe storage of hydrogen, as mentioned above, is also a prerequisite for the introduction of a Hydrogen Economy. In Table 1 hydrogen is compared with other fuels.

Fuel	Energy [kJ/g]	Energy [kJ/l]
Coal	**29.3**	**-**
Brown coal	**8.1**	**-**
Wood	**14.6**	**-**
Gasoline	**43.5**	**30590**
Diesel	**42.7**	**29890**
Methanol	**19.6**	**15630**
Natural gas	**50.02**	**31.7**
Hydrogen	**119.9**	**10**

Table 1. Hydrogen, in comparison with conventional fuels.

In comparison with the conventional fuels, Table 1 clearly reveals that hydrogen has a high energy content per unit mass, but a low energy content per unit volume. This, therefore, demands a special storage technique for hydrogen, especially for traction applications.

7. Storage of Hydrogen

Hydrogen can be stored in different forms and mainly three ways of storage are distinguished, i.e., storage in high-pressure tanks, storage by means of liquefaction, or by absorption in a metal lattice, forming a metal hydride. Here, a distinction needs to be made between centralised or decentralised use of hydrogen. In the case of decentralised use of hydrogen, i.e., in emission-free vehicles, it should be realised that containing the lightest gas in the universe on board a car presents an enormous challenge. For a normal-size fuel cell powered car with an average driving range of 500km, about 6kg (6wt%) of hydrogen needs to be stored on board. At atmospheric pressure, the energy density per unit volume of hydrogen gas is about 3000 times smaller than that of gasoline, so even novel fibre-reinforced gas cylinders containing hydrogen compressed to 800 bars are not sufficient and take up too much space. To date, high-pressure gas cylinders are used in the fuel cell buses in participating European Capital Cities and sponsored by the EU Clean Urban Transport in Europe (CUTE) program. Within this program three of these emission-free buses are in operation in Amsterdam. For private cars, this storage option is not realistic. Liquefied hydrogen needs to be stored at -253ºC (20K), which requires extremely well insulated and, therefore, very expensive storage tanks. BMW, however, has selected this storage option for developing emission-free vehicles.
An option that attracts global attention is absorption in a metal or an alloy. In the absorption process a solid solution (MH_x) is formed first. Subsequently a compound (MH_y) is formed according to the reaction,

$$MH_x + \tfrac{1}{2}(y - x)\, H_2 \rightarrow MH_y \qquad (9)$$

During the formation of the compound a plateau occurs in the phase diagram of the metal-hydrogen system, as is schematically presented in Figure 7.

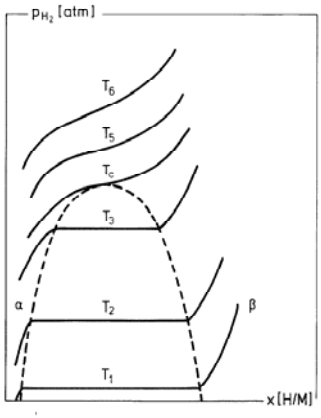

Figure 7. The hydrogen pressure – metal hydride composition diagram.

The formation of the metal-hydride compound is exothermic and the release is endothermic. While this contributes to safety of this storage system, it also means a loss of energy. Suitable storage materials should not require too high temperatures for hydrogen release and should not exhibit too high plateau pressures. In a comparison of hydrogen storage methods, it becomes clear that the concentration of hydrogen in metal hydrides is larger than in pressurized or liquid hydrogen, i.e., Table 2,

Compound	Hydrogen content [wt%]	H-atoms / unit volume [10^{22} cm^{-3}]	Density [kg/m^3]
H_2O	11	30	1000
liq. CH_4	25	6	425
H_2 (g), 150 atm	100	0.7	12
H_2 (l), 20 K	100	4.3	71
Graphite	4	-	-
C-nanotubes	<1	-	-
TiH_2	4	9	3800
MgH_2	7.6	6.5	-
LaH_3	2.1	6.5	-
$LaNi_5H_6$	1.4	5.5	6225
$TiFeH_2$	1.9	6	5470

Table 2. Comparison of hydrogen storage methods.

For M-H_2, the systems Fe-Ti-H and La-Ni-H have been studied widely. With a storage capacity of less than 2 wt% hydrogen, these alloys are too heavy for mobile applications. Therefore, the system Mg-H is being studied as it can store up to 7.6 wt% of hydrogen. The kinetics of hydrogen absorption and desorption of this system are slow though, but can be improved substantially by decreasing the grain size of the Mg particles to the nano-size regime. Furthermore, the addition of small amounts (<1%) of nano-sized transition metal oxide catalysts.

8. Conclusions

Nano-structured functional materials for non-silicon based solar cells have furthered the pace of advanced in developing advanced and novel solar cells. The dye-sensitized Grätzel solar cell has stimulated the development of novel cheap 3D nano-structured solid-state solar cells. Atomic Layer Deposition and Aerosol Spray Pyrolysis are instrumental for this development. The presently achieved conversion efficiencies of about 5% show, that this type of solar cells represents a promising concept. It is anticipated that these 3D solar cells will reach efficiencies of over 8% in the coming years and will start to replace expensive silicon-based solar cells. Nano-structured transition metal oxide catalysts improve the kinetics of hydrogen sorption in especially nano-structured Mg-based hydrides. The mechanism is not yet understood, but enhanced point defect densities in these nano-structured metal oxide catalysts play an important role.

9. References

1. *The Wall Street Journal Europe* (2004) Vol. XXII, No.144, August 25, page A1.
2. Shell International (2001), Energy needs, choices, and possibilities, scenarios to 2050. London.
3. A. Merkel, The role of science in sustainable development. Science **281**, www.sciencemag.org
4. L. Reijnen, Gas-Phase Synthesis of Sulfide Absorbers for Thin-Film and Nanostructured Solar Cells. Ph.D.Thesis, Delft University of Technology, Delft, The Netherlands. (2003). ISBN 90-6734-295-5.

5. C.L. Zilverentant, Hybrid Solar Cells of Titanium Dioxide Sensitized with Organic Semiconductors. Ph.D.Thesis, Delft University of Technology, The Netherlands. (2003). ISBN 90-9017-529-6.
6. A. Jaeger-Waldau, Status of Thin-Film Solar Cells in Research, Production and Market, Solar Energy 77 (2004) 667-678.
7. M. Grätzel, Photo-electrochemical Cells, Nature 415 (2001) 338-344.
8. A. Fujishima and K. Honda, Electrochemical photolysis of water at a semiconductor electrode, Nature 238 (1972) 37-38.
9. A. Mackor and J. Schoonman, Thin-film dye sensitization and impurity effects on TiO_2 and $SrTiO_3$ electrodes for the photoelectrolysis of water, Recl. Trav.Chim. Pays-Bas 99 (1980) 71-72.
10. O'Regan and M. Grätzel, A low-cost, high efficiency solar cell based on dye-sensitized colloidal TiO_2 films, Nature 353 (1991) 737-740.
11. M. Grätzel, Properties and applications of nanocrystalline electronic junctions, in H.S. Nalwa (ed.) Handbook of Nanostructured Materials and Nanotechnology, Vol. 3: Electrical Properties, Academic Press, ISBN 0-12-513763-X.
12. M. Grätzel, Private Communication, (2004).
13. C.L. Huisman, A. Goossens and J. Schoonman, Preparation of a nanostructured composite of titanium dioxide and polythiophene: a new route towards 3D heterojunction solar cells. Synthetic Metals 138 (2003) 237-241.
14. C.L. Huisman, Functional ceramics for organic solar cells, Klei, Glas en Keramiek, Jaargang 24, Nr. 2 (2003) 23-27.
15. R. van de Krol, private communication and D. Perniu, M. Nanu, R. van de Krol, and J. Schoonman, Nano- structured materials for a Hydrogen Economy, in A. Vaseashta, D. Dimova-Malinovska, and J.M. Marshall (eds.) Nanostructured and Advanced Materials for Applications in Sensor, Optoelectronic and Photovoltaic Technology, Springer, Dordrecht, The Netherlands, (2005) 251-258.
16. K. Ernst, A. Balaidi, and R. Könekamp, Solar cell with extremely thin absorber on highly structured substrate, Semicond. Sci. Technol. 18 (2003) 475-479.
17. M. Nanu, L. Reijnen, B. Meester, A. Goossens, and J. Schoonman, $CuInS_2$-TiO_2 hetero-junction solar cells obtained by atomic layer deposition, Thin Solid Films 431-432 (2003) 492-496.
18. M. Nanu, J. Schoonman, and A. Goossens, Inorganic nano-composites of n- and p-type semiconductors: a new type of three-dimensional solar cell, Adv. Mater. 16 (2004) 453-456.
19. C.L. Huisman, J. Schoonman, and A. Goossens, The application of inverse titania opals in nano-structured solar cells, Solar Energy Mater. & Solar Cells 85 (2005) 115-124.
20. J. Schoonman, Nanostructured materials for the conversion of sustainable energy. In ref. 15, 271-280.
21. C.S. Enache, J. Schoonman, and R. van de Krol, The photoresponse of iron- and carbon-doped TiO_2 (anatase) photoelectrodes, J. Electrocer. 13 (2004) 177-182.
22. R. Asahi, T. Morikawa, T. Ohwaki, K. Aoki, and Y. Taga, Visible-Light Photocatalysis in Nitrogen-doped Titanium Oxides, Science 293 (2001) 269-271
23. W. Oelerich, T. Klassen, and R. Bormann, Metal oxides as catalysts for improved hydrogen sorption in nanocrystalline Mg-based materials, J. Alloys Compounds 315 (2001) 237-242.